Getting the Most out of Your 2D Mass Spectrum: Isotopic Distributions and Fragmentation Pathways

Maria A. van Agthoven[1]; Federico Floris[1]; Mark P. Barrow[1]; Christopher Wootton[1]; Lionel Chiron[5]; Marie-Aude Coutouly[3]; Marc-André Delsuc[2,3,5]; Christian Rolando[4] & Peter B. O'Connor[1]

1) University of Warwick, Coventry, UK; 2) IGBMC, Illkirch-Graffenstaden, France; 3) NMRTEC, Illkirch-Graffenstaden, France; 4) Université de Lille, Sciences et Technologies; 5) CASC4DE, Illkirch-Graffenstaden, France

See also:
Poster MP209
Talk TOA 2:30 pm
For 2D mass spectrometry news on Twitter, follow: @2D_FT_ICR_MS

Overview

- We investigate the isotopic distributions for fragmentation peaks for large molecules in a 2D FT-ICR mass spectrum.
- We measure the radius of the fragmentation zone in IRMPD for different excitation pulse conditions.
- We break down the fragmentation profile by fragment in order to see how fragmentation pathways affect the 2D mass spectrum, and how 2D mass spectra can be used to study fragmentation pathways.

Principle of 2D FT-ICR MS

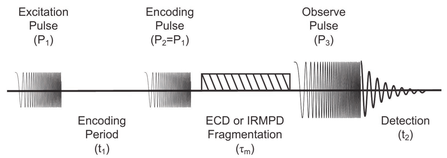

Figure 1: Pulse sequence for two-dimensional FT-ICR MS.

The pulse sequence of this experiment is shown in Fig. 1 [1-11].

- Precursor ions are excited coherently from the center of the ICR cell by the **excitation pulse** P_1.
- During the **encoding period** t_1, precursor ions rotate at their own cyclotron frequency. At the end of t1, they have accumulated a phase $\omega_{ICR} \times t_1$.
- The **encoding pulse** P_2 changes the precursor ions' radius according to their phase: if ion motion is in phase with the closest excitation plate , ions are coherently excited, if ion motion is out of phase with the closest excitation plate, ions are coherently de-excited.

At the end of P_2, ion cyclotron radii are modulated according to cyclotron frequency and t_1.

- A period of **radius-dependent fragmentation** (IRMPD, ECD, CID…) produces fragment ions with abundances that are dependent on the cyclotron radii of their precursors, i.e. their cyclotron frequency and t_1.
- The **observe pulse** P_3 excites both precursor and fragment ions in order to measure the transient (detection date t_2).

Transients are recorded with regularly incremented values of t_1. A double Fourier transform according to t_1 and t_2 shows correlations between precursors and fragments in a two-dimensional map.

After mass calibration the 2D mass spectrum can be read with precursor m/z ratios vertically and fragment m/z ratios horizontally (fig. 2). 2D mass spectra show several characteristic lines :

- **The autocorrelation line** ($y = x$) shows the correlation of the prescursor ion signal with their own cyclotron radius.
- **Horizontal fragment ion spectra** ($y = m_{precursor}$) show the fragmentation patterns of each precursor ion (figs 2d and 2e).
- **Vertical precursor ion spectra** ($x = m_{fragment}$) show the precursor ions of each fragment ion (fig. 2f).
- **Electron capture lines** ($y = (n\text{-}p)*x/n$) show the capture of p electrons by n-charged precursor ions.
- **Neutral loss lines** ($y = x + m_{neutral}$) show the loss of neutrals by precursor ions (figs. 2g, 2h, 2i) .

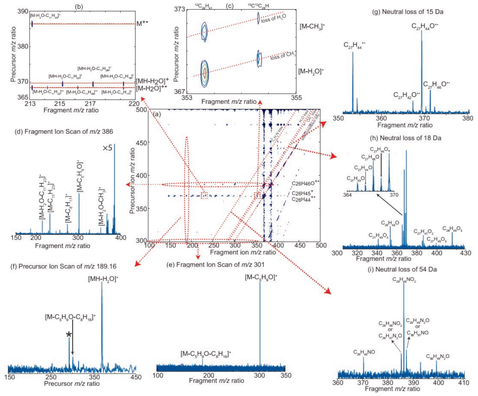

Figure 2: (a) APPI 2D IRMPD FT-ICR mass spectrum of cholesterol. Expanded regions: (b) *m/z* 213-220 horizontally and *m/z* 365-390 vertically and (c) *m/z* 353-355 horizontally and *m/z* 367-373 vertically. Profiles: (d) Fragment ion scan of *m/z* 386. (e) Fragment ion scan of *m/z* 301. (f) Precursor ion scan of *m/z* 189.16. * Harmonic peak from *m/z* 369. (g) Neutral loss scan for a loss of 15 Da. (h) Neutral loss scan for a loss of 18 Da. (i) Neutral loss scan for a loss of 54 Da. *^{13}C isotope peak distorted by scintillation noise from the precursor peak of *m/z* 369 [11].

Isotopic Distributions in 2D Mass Spectra

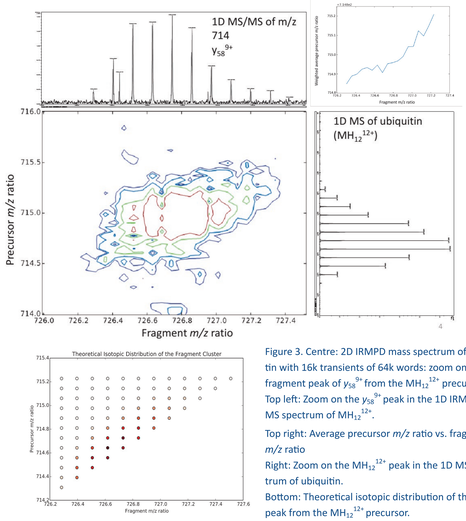

Figure 3. Centre: 2D IRMPD mass spectrum of ubiquitin with 16k transients of 64k words: zoom on the fragment peak of y_{58}^{9+} from the MH_{12}^{12+} precursor.
Top left: Zoom on the y_{58}^{9+} peak in the 1D IRMPD MS/MS spectrum of MH_{12}^{12+}.
Top right: Average precursor *m/z* ratio vs. fragment *m/z* ratio
Right: Zoom on the MH_{12}^{12+} peak in the 1D MS spectrum of ubiquitin.
Bottom: Theoretical isotopic distribution of the y_{58}^{9+} peak from the MH_{12}^{12+} precursor.

- With increasing compound mass, the isotopic distribution shifts towards heavier isotopologues.
- During fragmentation, there is a redistribution of of isotopes (Fig. 3).
- The probabilitiy p(A/B) for precursor isotopologue B (with probability p(B)) to dissociate into fragment isotopologue A (with probability p(A)) and mirror fragment isotopologue B-A (with probability p(B-A)) is (Fig. 3 bottom):

$$p(A/B) = \frac{p(A) \times p(B-A)}{p(B)}$$

- Neutral loss lines and dissociation lines can only be measured accurately along constant isotope lines (same number of ^{13}C, ^{15}N, ^{17}O, ^{18}O, ^{2}H and ^{34}S in both the precursor and the fragment).
- **An accurate representation of 2D isotopic patterns is important for both fragment and precursor mass measurements in 2D mass spectra.**

Fragmentation Pathways in 2D Mass Spectra

- de Koning's ion excitation model in an Infinity cell [4] (B is the magnetic filed, V_{pp} the RF excitation voltageamplitude, T_{exc} the length of the excitation pulse, and d the diameter of the ICR cell):

$$r(ion) = \frac{0.9 V_{pp} T_{exc}}{2Bd}$$

- By measuring the fragmentation efficiency as a function of V_{pp} (Fig. 4), the size of the fragmentation zone can be estimated [10].
- The actual measurement (Table 1) is inconsistent with the manufacturer's specifications (~3 mm) and increases with pulse length, **which suggests that at short pulse length there is significant off-resonance excitation.**

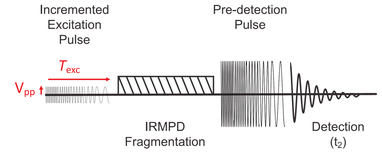

Figure 4: Pulse sequence for fragmentation zone measurements [10].

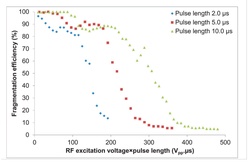

T_{exc} (µs)	Measured radius of fragmentation zone (µm)
2.0	94
5.0	134
10.0	188

Figure 5: Fragmentation efficiency measurement of angiotensin I vs. RF excitation voltage times pulse length.

Table 1: Estimated radius of the fragmentation zone for each pulse length using the de Koning model.

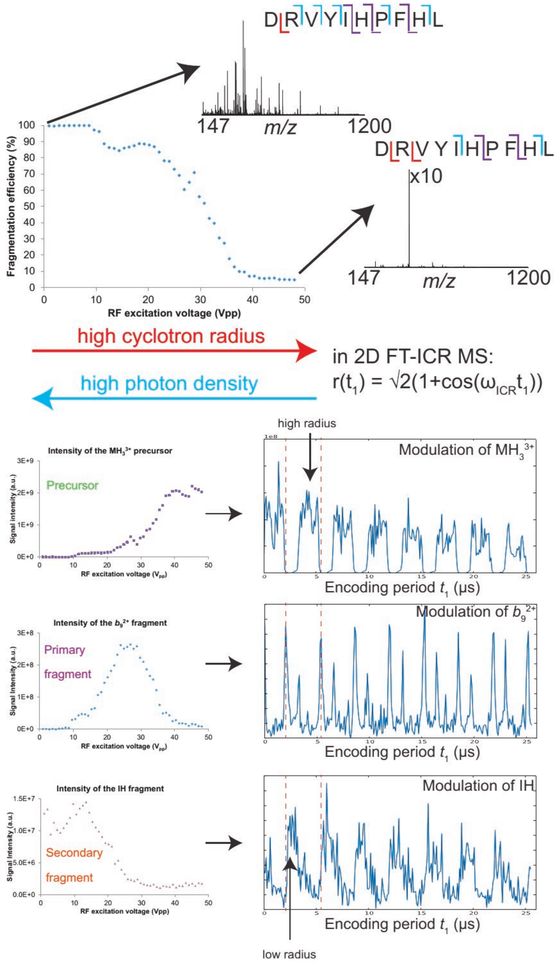

Figure 6: Fragmentation efficiency of MH_3^{3+} of angiotensin I vs. RF excitation voltage and expansion into MS/MS spectra. Signal intensity vs. RF excitation voltage for MH_3^{3+}, b_9^{2+} and IH^+. The shape of the fragmentation zone is different for each ion species, which translates into different types of modulation along t_1 in the 2D FT-ICR experiment (see Fig. 1).

- The fragmentation pattern of MH_3^{3+} of angiotensin I is very different at low radius (high photon density) than at high radius (low photon density).
- The intensity profiles for MH_3^{3+} and fragments are different, but they are also different for primary and secondary fragments.
- b_9^{2+} is a primary fragment that is formed at low photon density (high radius) but re-fragments if the photon density is high enough (low radius).
- IH^+ is a secondary fragments that is formed by refragmentation of primary fragments at high photon density (low radius).
- In 2D FT-ICR MS, the cyclotron radius of precursor ions is modulated according to t_1 (see Fig. 1). Since the fragmentation efficiency in IRMPD is radius-dependent, this means that the intensity of each ion species (precursor and fragment) is modulated according to t_1.
- The intensity profiles of MH_3^{3+} and IH^+ are the mirror image of each other, so their fragmentation modulations are similar square-looking yet phase-shifted by 180°.
- The intensity profile of b_9^{2+} is Gaussian-like and centered around ~25 V_{pp} excitation voltage. The resulting modulation has a Dirac comb-like shape that has two maxima per cyclotron period.
- In the 2D mass spectrum this translates into phase shifts (between precursors and fragments that are formed at the lowest radius, like IH^+) and different harmonicities (for fragments that are not present at the lowest radius, like b_9^{2+}).
- **This phenomenon can be reverse-engineered in order to determine the fragmentation profile of each fragment and whether fragment is a primary or secondary fragment.**
- **The fragmentation pattern in a 2D mass spectrum is different than in an MS/MS spectrum because it is a composite of all MS/MS spectra over a range of fragmentation conditions.**

Experimental Methods

- All experiments were performed on a 12 T Bruker solariX FT-ICR mass spectrometer
- Ion source: positive nanospray (ubiquitin, angiotensin I) and APPI (cholesterol)
- Fragmentation mode: IRMPD using a 10.6 µm, 25 W CO_2 laser
- Datasets (pulse sequence: see Fig. 1): 2048×128k datapoint transients (1GB) with *m/z* 100-500 (cholesterol), 16k*64k datapoint transients (4 GB) with *m/z* 147-3000 (ubiquitin), 256*4M datapoint transients (4GB) with *m/z* 147-1500 and quadrupole isolation at *m/z* 433 (angiotensin I)
- MS/MS spectra (pulse sequence: see Fig. 4): 20 scans of 4M word transients with *m/z* 147-1500 and quadrupole isolation at *m/z* 433 (angiotensin I)

Conclusions

- For large molecules, fragmentation peaks can be shifted towards higher masses because of 2D isotopic distributions, which we can predict.
- Fragmentation patterns in 2D mass spectra cover all fragmentation conditions within the fragmentation zone, whereas MS/MS spectra only represent one fragmentation condition.
- From 2D mass spectra it is possible to obtain the fragmentation profile of each fragment of a single precursor.

Acknowledgments

The authors thank the Department of Chemistry of the University of Warwick and the EPSRC for funding this research (grant nr: EP/J000302/1).

EPSRC Pioneering research and skills

References:

1. A.G. Marshall et al., *Chem. Phys. Letts.* 105 (1984) 233-236.
2. P. Pfändler et al., *J. Am. Chem. Soc.* 110 (1988) 5625-5628.
3. Guan. et al. *J. Chem. Phys.* 91 (1989) 5291-5295.
4. De Koning et al. *Int. J. Mass Spectrom. And Ion Process* 165/166 (1997) 209-219.
5. M.A. van Agthoven et al., *Int. J. Mass Spectrom.* 306 (2011) 196-203.
6. M.A. van Agthoven et al., *Rapid Commun. Mass Spectrom.* 25 (2011) 1609–1616.
7. M.A. van Agthoven et al. *Anal. Chem.* 84 (2012) 5589–5595.
8. M.A. van Agthoven et al. *Anal. Bioanal. Chem.* 405 (2013) 51-61.
9. L. Chiron et al., *Proc. Natl. Acad. Sci. U. S. A.* 111 (2014) 1385-1390.
10. M.A. van Agthoven et al., *Int. J. Mass Spectrom.* 370 (2014) 114-124.
11. M.A. van Agthoven et al. *J. Am. Soc. Mass Spectrom.* article in press.